A FAST PROPAGATING EXTREME-ULTRAVIOLET WAVE ASSOCIATED WITH A MINI-FILAMENT ERUPTION

Ruisheng Zheng, Yunchun Jiang, Jiayan Yang, Yi Bi, Junchao Hong, Dan Yang, and Bo Yang
National Astronomical Observatories/Yunnan Astronomical Observatory, Chinese Academy of Sciences, Kunming 650011, China; zhrsh@ynao.ac.cn

ABSTRACT

The fast extreme-ultraviolet (EUV) waves (>1000 km s^{-1}) in the solar corona were very rare in the past. Taking advantage of the high temporal and spatial resolution of the *Solar Dynamics Observatory* observations, we present a fast EUV wave associated with a mini-filament eruption, a C1.0 flare, and a coronal mass ejection (CME) on 2011 September 30. The event took place at the periphery between two active regions (ARs). The mini-filament rapidly erupted as a blowout jet associated with a flare and a CME. The CME front was likely developed from the large-scale overlying loops. The wave onset was nearly simultaneous with the start of the jet and the flare. The wave departed far from the flare center and showed a close location relative to the rapid jet. The wave had an initial speed of about 1100 km s^{-1} and a slight deceleration in the last phase, and the velocity decreased to about 500 km s^{-1}. The wave propagated in a narrow angle extent, likely to avoid the ARs on both sides. All the results provide evidence that the fast EUV wave was a fast-mode MHD wave. The wave resisted being driven by the CME, because it opened up the large-scale loops and its front likely formed later than the wave. The wave was most likely triggered by the jet, due to their close timing and location relations.

Key words: Sun: activity – Sun: corona – Sun: filaments, prominences

Online-only material: animation, color figures

1. INTRODUCTION

Extreme-ultraviolet (EUV) waves were first observed by the EUV Imaging Telescope (EIT) on board the *Solar and Heliospheric Observatory* (*SOHO*) spacecraft (e.g., Moses et al. 1997; Thompson et al. 1998); hence, they were originally referred to as "EIT waves." EUV waves generally appear as large-scale, diffuse, single-pulse coronal enhanced transients. They normally emanate from flaring and eruptive active regions (ARs) and subsequently propagate outward into the quiet Sun over significant distances. They tend to avoid ARs and stop near the separatrix between ARs or at the boundaries of coronal holes (Thompson et al. 1998, 1999; Wills-Davey & Thompson 1999; Wu et al. 2001; Li et al. 2012). More and more evidence demonstrates that EUV waves are intimately associated with coronal mass ejections (CMEs; or other types of mass motions) rather than with flares (Biesecker et al. 2002; Cliver et al. 2005; Chen 2006; Zheng et al. 2012).

Since their discovery, the physical nature of EUV waves has been a subject of strong debate. There are some competing models, such as coronal fast-mode magnetohydrodynamic (MHD) waves (e.g., Thompson et al. 1999; Wang 2000; Wu et al. 2001; Ofman & Thompson 2002; Long et al. 2008; Gopalswamy et al. 2009; Veronig et al. 2010), slow-mode or soliton-like waves (Wills-Davey et al. 2007; Wang et al. 2009), pseudo-waves related to a current shell or successive restructuring of the magnetic field associated with the CME expansion (Delannée et al. 2008; Attrill et al. 2007), and hybrid models including both wave and pseudo-wave scenarios (Chen et al. 2002; Zhukov & Auchère 2004; Cohen et al. 2009; Liu et al. 2010; Downs et al. 2011; Cheng et al. 2012). For details of observations and models, please refer to recent reviews (Wills-Davey & Attrill 2009; Gallagher & Long 2011; Warmuth 2010; Zhukov 2011).

EUV waves are usually detected propagating at speeds of several hundred km s^{-1}. According to the model of fast-mode MHD waves, the wave speed could be up to 1000–2000 km s^{-1},

in the range of Alfvén speed (Wills-Davey et al. 2007). The fast waves have been theoretically predicted and simulated (e.g., Bogdan et al. 2003; Fedun et al. 2011; Ofman et al. 2011). However, waves with speeds of >1000 km s^{-1} are rarely observed. There are only several super-fast fast-mode waves with speeds of about 2000 km s^{-1}, but they are a different type of wave localized in a closed loop or in a magnetic funnel (Williams et al. 2002; Liu et al. 2011).

In this paper, using the high-cadence and sensitivity observations from the Atmospheric Imaging Assembly (AIA; Lemen et al. 2011) on the *Solar Dynamics Observatory* (*SDO*), combined with the observations from Extreme Ultraviolet Imager (EUVI; Howard et al. 2008) on board the twin spacecrafts of *Solar Terrestrial Relations Observatory* (*STEREO*; Kaiser et al. 2008), we concentrate on a very fast EUV wave associated with a mini-filament eruption on 2011 September 30.

2. OBSERVATIONS AND DATA ANALYSIS

On 2011 September 30, a fast EUV wave emanated from the periphery between two ARs. It was associated with a mini-filament eruption, a C1.0 flare, and a weak CME. The eruption center is identified at the location of $x = 490''$, $y = 130''$, measured from the solar disk center. We mainly use the observations from AIA on the *SDO*. The AIA has 10 EUV and UV wavelengths, covering a wide range of temperatures. The cadence is up to 12 s, and the pixel resolution is $0''.6$. The wave is strongest in 193 Å and is also visible in 211 and 335 Å. In order to analyze the dynamics of the waves, we employ a time-slice approach in which the slices start from the identified eruption center and have a length of $600''$. In addition, the observations from the EUVI and Inner Coronagraph (COR1) on the *STEREO* Ahead (-A) are utilized to study the evolution of the associated CME. To check the filament morphology before its eruption, we use full-disk Hα filtergrams from the Global Oscillation Network Group (GONG) at the National Solar Observatory
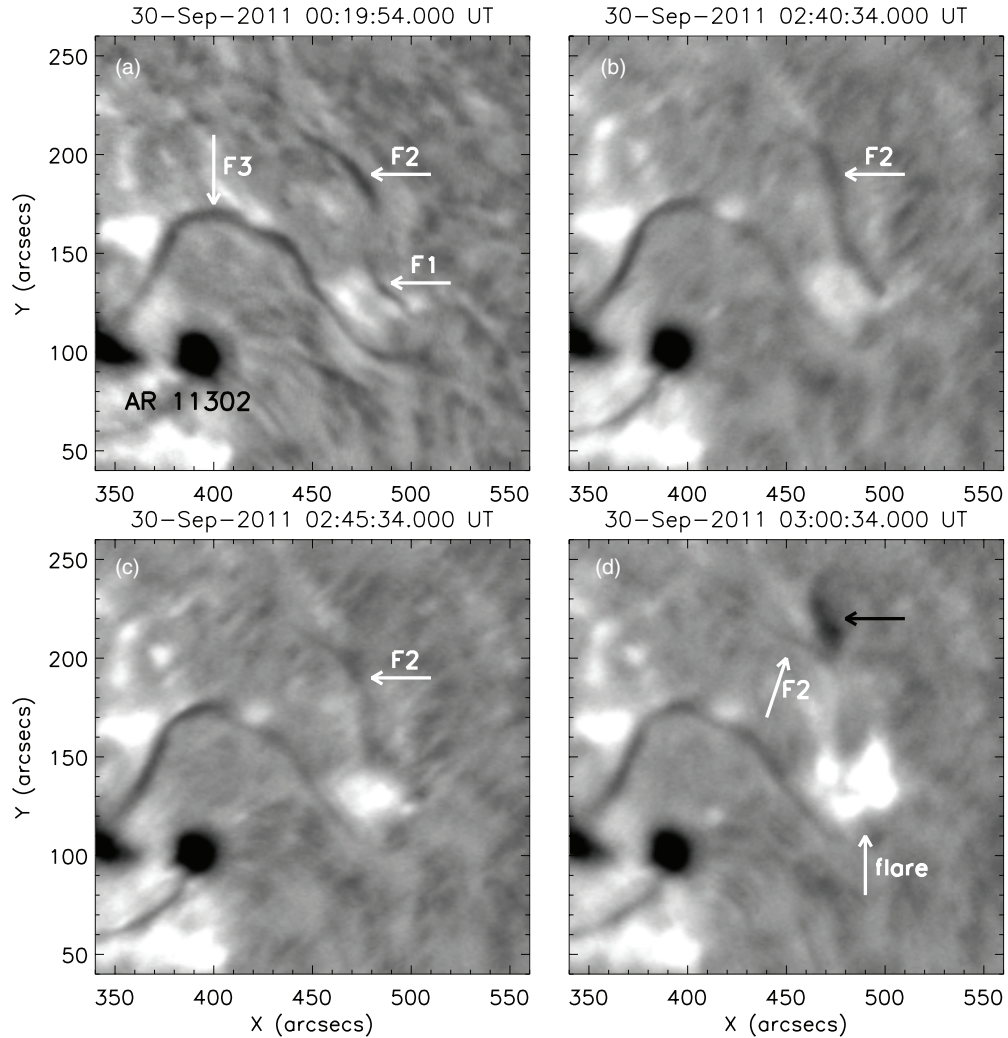
Figure 1. Evolution of the filament before, during, and after the eruption in Hα filtergrams from the GONG/NSO. F1 is the erupted filament with which we are concerned; F2 and F3 are two nearby filaments. The black arrow in panel (d) indicates the falling material of F1.

(NSO). All the images are differentially rotated to a reference time (about 02:40:00 UT).

3. RESULTS

3.1. Mini-Filament Eruption

The Hα line center observations from the GONG/NSO before, during, and after the filament eruption are shown in Figure 1. In panel (a), the eruptive filament (F1) was about 40″, the typical length of a mini-filament. A bigger filament (F2) is in the north and a large filament (F3) is in the east AR 11302. F1 and F2 were likely in the same filament channel. Before the eruption, F1 was activated and became darker and darker, so it seemed that F1 was connected to F2 (panel (b)). F1 was very faint during its rise phase (panel (c)). The detailed eruption process was missed due to the lower cadence. Accompanying the eruption, a C1.0 flare occurred and only appeared around the location of F1, which provided the evidence that only F1 erupted (panel (d)). Due to the bright flaring, the eruptive material could not be seen clearly, and F2 also became very faint. F2 and F3 survived during the eruption. Note that a black patch formed (the black arrow in panel (d)); this was the remains of F1, ejected there during the eruption.

The coronal response for the eruption is shown in detail in high-quality images of AIA 304 (upper panels) and 193 Å (middle panels) in Figure 2. Before the eruption, three filaments were very evident, and F1 was independent of F2 (panel (a)). When F1 was rising, it consisted of the bright north part and the dark south part (panels (b) and (d)). During the eruption, the south part was ejected rapidly as a curtain-like jet (white arrows in panels (c) and (e)), similar to the blowout jet (Hong et al. 2011; Shen et al. 2012) recently defined in Moore et al. (2010). It is interesting that some material was expelled northward (black arrows in panels (c) and (e)). In the source region, two flare ribbons lay on both sides of the filament channel of F1. After the eruption, the post-flare loops connected the flare ribbons, and there was some dark mass north of the eruption center (the black arrow in panel (f)). F2 and F3 survived, and the ambient AR loops remained nearly intact during the eruption (panels (e) and (f)).

The bottom panels show the eruption in EUVI-A 304 Å images from the limb view, which is helpful to well understand the eruption. F1 was dragged obliquely down and disrupted from the middle. The north part became bright and the south was bent like an arc, while F2 remained in place (panel (g)). The north part bounced northward and fell back to the surface (the black arrow in panel (h)), consistent with the black patch
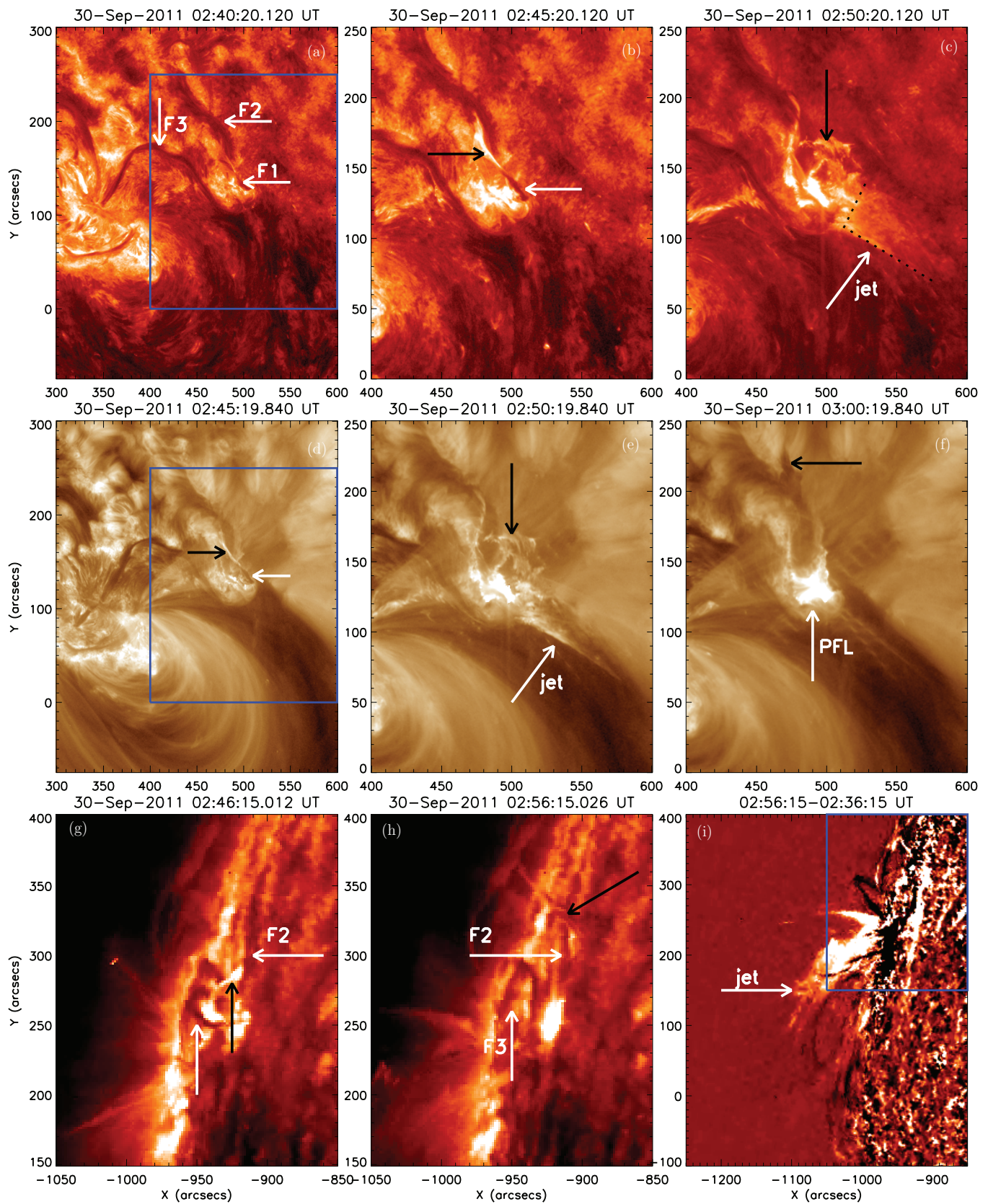
Figure 2. Eruption shown by images in AIA 304 (upper) and 193 Å (middle) and in EUVI-A 304 Å. The black arrows point to the part of F1 that was falling back during the eruption. The blue box indicates the FOV of the other two panels in each row.

(A color version of this figure is available in the online journal.)

3
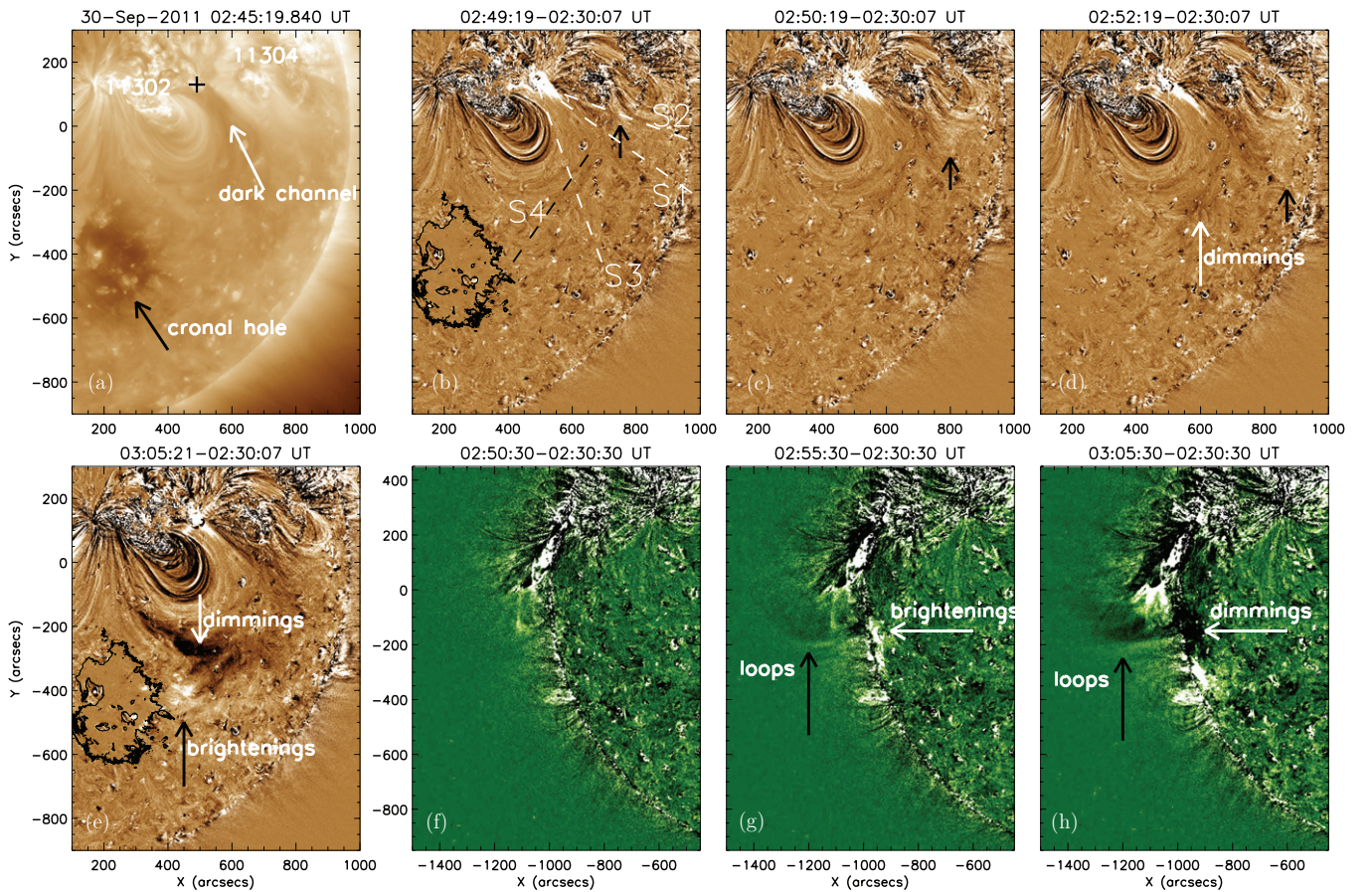
Figure 3. Sequential base difference images in AIA 193 Å (panels (a)–(e)) and EUVI 195 Å (panels (f)–(h)) displaying the evolution of the wave. The plus in panel (a) represents the eruption center, and the black contours in panels (b) and (e) indicate the boundary of the coronal hole. The short black arrows in panels (b)–(d) point to the wave front, and the sectors in panel (b), S1–S4, are used to obtain the time-slice images in Figure 4.

(An animation and a color version of this figure are available in the online journal.)

in panel (f) and in Figure 1. The south arc was ejected rapidly as a jet. The bright jet was shown more clearly in a larger field of view (FOV) in a difference image (panel (i)). Of course, F2 and F3 also survived during the eruption from the limb view (panel (h)).

3.2. Fast EUV Wave

The filament eruption was closely associated with an EUV wave, which is shown in two perspectives from AIA and EUVI-A in Figure 3. Panel (a) exhibits the general view of the eruption environment. The eruption region (centered at the plus) was between ARs 11302 and 11304, and there was a coronal hole southeast of AR 11302. Between the bright loops of the two ARs, there was a dark coronal channel (the white arrow), indicating a lower density. The wave emanated from the eruption center at about 02:47 UT, looking like it was pushed by the jet. It propagated along the dark channel in a narrow angle extent, seemingly avoiding the AR loops on both sides. The wave was weak (see the attached movie diffwave_193.mpg); its front is indicated by black arrows in panels (b)–(d). At the same time, there began to appear loop-like dimmings (the white arrow in panel (d)) connecting the eruption region and the quiet region in the southeast. This indicates that there were likely large-scale exploded overlying loops generated by the filament eruption. As time went on, the dimmings became deeper and deeper in the southeast, and some brightenings appeared on the edge of the dimmings, close to the coronal hole (black

contours). In addition, the alternating bright and dark loops in AR 11302 indicated the oscillation of the clusters of loops during the eruption, which was better seen in 171 Å. Next, we examine the wave in the limb view from the EUVI-A. Maybe the wave was weak and fast, as it was very faint in the low-cadence images of EUVI-A 195 Å. However, the expansion of the overlying loops is very evident (black arrows in panels (g) and (h)). It is interesting that the south end of the loops was nearly fixed during the eruption. Around the loop end, there were deep dimmings, and some brightenings appeared on the edge of the dimmings, consistent with the situation in panel (e). It is plausible that the loop expansion in the direction was stopped near the coronal hole, which resulted in the brightenings as a result of the compression. Due to the continued radial expansion, the dimmings were deeper and deeper.

To best display the kinematics of the EUV wave, we employ the time-slice approach and analyze the evolution of the wave front along the selected sectors (S1–S4). The angles of S1–S3 are 235°, 250°, and 200°, respectively, counted counterclockwise from the north (white dashed lines in Figure 3(b)). S1 and S2 are in the ejection direction of the jet, and S3 deviates from the ejection direction. Due to the influence of the clusters of loops in AR 11302, we chose a special sector (S4) to study the wave propagation toward the coronal hole (the black dashed line in Figure 3(b)).

Figure 4 displays the propagation of the wave in S1–S4. In S1 and S2, the wave set off at about 02:47 UT, close to the onsets of the flare and the jet. The wave front appeared as bright oblique
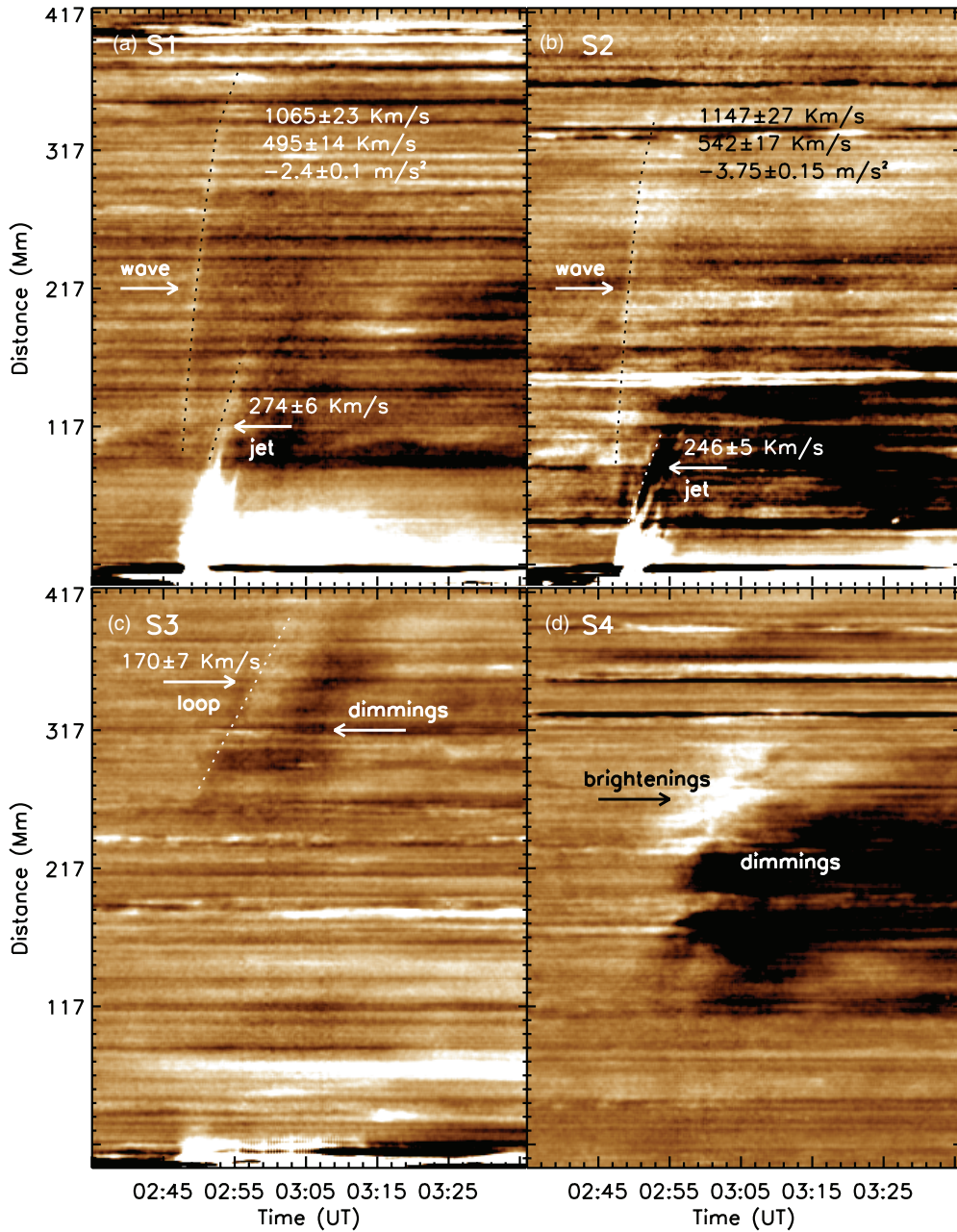
Figure 4. Base difference time-slice images obtained from the sectors S1–S4 in 193 Å. The velocities and accelerations of the wave are attached above.
(A color version of this figure is available in the online journal.)

stripes, and its start point was at a distance of about 100 Mm from the flare center but was just ahead of the blowout jet. The wave was likely intimately associated with the jet. Intriguingly, the wave had a very fast initial velocity of about 1100 km s^{-1} and propagated up to a distance of 300 Mm in 6 minutes. The wave front revealed a decelerating character, and the speed decreased to about 500 km s^{-1} in the last phase. The speed of the jet was only about 270 km s^{-1}. In S3, there was no sharp wave front, but a diffuse oblique stripe followed by faint dimmings far from the source region. It did not represent the wave but the loops of the associated CME, namely, the proposed large-scale overlying loops. The loops began to expand at about 02:49 UT, later than the wave onset, and had an expansion speed of about 170 km s^{-1}. In S4, the wave was also not seen. This is consistent with the situation in Figure 3. The wave was likely avoiding the ARs and could not propagate toward the southeast coronal hole. The

wave only propagated in a narrow angle range, dominated along the dark channel. There were deep long-duration dimmings and some brightenings on the periphery, consistent with the halt of the proposed large-scale overlying loops.

3.3. CME

The coronagraphs on the *STEREO* detected a faint CME associated with the filament eruption, shown by composite images of inner EUVI-A 195 Å with outer COR1-A images in Figure 5. The CME first appeared in the COR1 FOV at about 03:00 UT and perfectly connected with the south expansive loops (panel (a)). As the CME expanded, its downward lateral movement was halted by the open field lines nearby. As a result of the compression, the southern CME and the open field lines both became very bright and could be easily distinguished
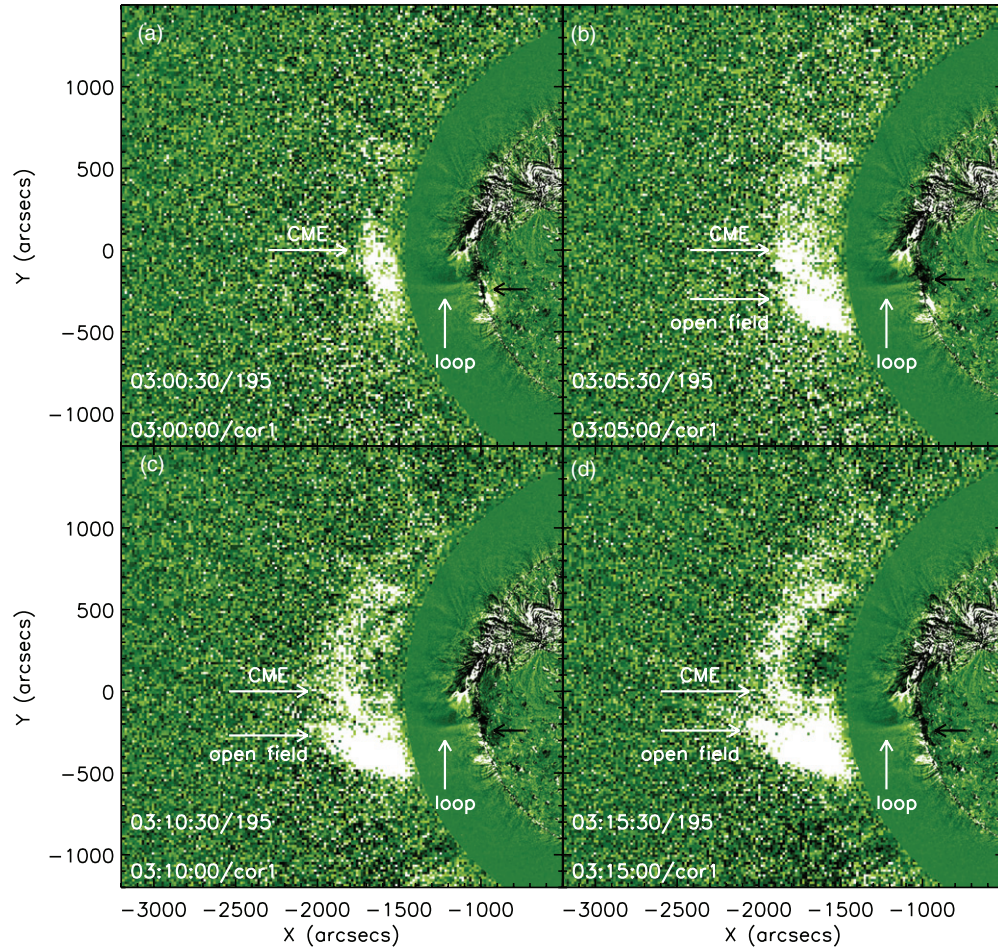
Figure 5. Composite images of inner EUVI-A 195 Å with outer COR1-A images, showing the CME evolution and the loops in the lower coronal. The black arrows indicate the dimmings and brightenings associated with the eruption.

(A color version of this figure is available in the online journal.)

(panels (b)–(d)). In addition, the south loops in EUVI FOV were visible all the time, and the long-duration dimmings and their associated brightenings were consistent with those in Figures 3 and 4 (black arrows). Thus, the lateral expansion of the CME was asymmetrical and mainly northward, but the northern CME was very faint. The CME propagated very slowly in the radial direction, with an estimated speed of 300 km s^{-1}.

4. DISCUSSION AND CONCLUSIONS

To check the magnetic field configuration for the eruption, we plot the potential magnetic field lines in the views from EUVI-A 195 Å (left panel) and from AIA 193 Å (right panel) in Figure 6, extrapolated from the Potential Field Source-Surface model (Schrijver & De Rosa 2003) with the *SOHO*/Michelson Doppler Imager magnetogram (Scherrer et al. 1995). The blue lines represent the large-scale overlying loops, and the white lines denote the open field lines from the coronal hole. They are consistent with the dimmings and brightenings. The filament eruption occurred under the large-scale overlying loops. The loop expansion was stopped near the open field lines from a coronal hole, which resulted in remote deep dimmings and brightenings.

Combining the observations from the *SDO*/AIA, the *STEREO*/EUVI-A and cor1-A, and the GONG/NSO, we present a very fast EUV wave associated with a mini-filament

eruption on 2011 September 30. Our main findings are as follows: (1) The filament eruption formed a blowout jet, and some material fell back nearby. The eruption was associated with a C1.0 flare and a CME, and the CME front was likely developed from the large-scale overlying loops. The southward expansion of the loops was stopped near a coronal hole, forming deep long-duration dimmings and brightenings. (2) The wave onset was nearly simultaneous with the start of the jet and the flare and was likely earlier than that of the CME front. The wave occurred far from the flare center, just ahead of the jet. (3) The wave propagated in a narrow angle extent, indicating that the wave was likely avoiding the ARs on both sides. (4) The wave had a very fast initial speed of about 1100 km s^{-1}, in the range of the Alfvén speeds in ARs for fast-mode waves. The slight negative acceleration in the last phase is consistent with freely propagating fast-mode waves (Veronig et al. 2008, 2010; Long et al. 2008). All the results provide evidence that the fast EUV wave was a fast-mode MHD wave.

EUV waves could be interpreted as fast-mode MHD waves, but very fast MHD waves with velocities exceeding 1000 km s^{-1} are very rare. Taking advantage of the short-duration eclipse, Williams et al. (2002) first detected a fast wave with a speed of 2100 km s^{-1} in a closed loop. With high-quality AIA data, Liu et al. (2011) first analyzed a quasi-periodic fast MHD wave with a speed of 2200 km s^{-1} in a magnetic funnel, driven by the quasi-periodic flare. The wave fronts were only visible in
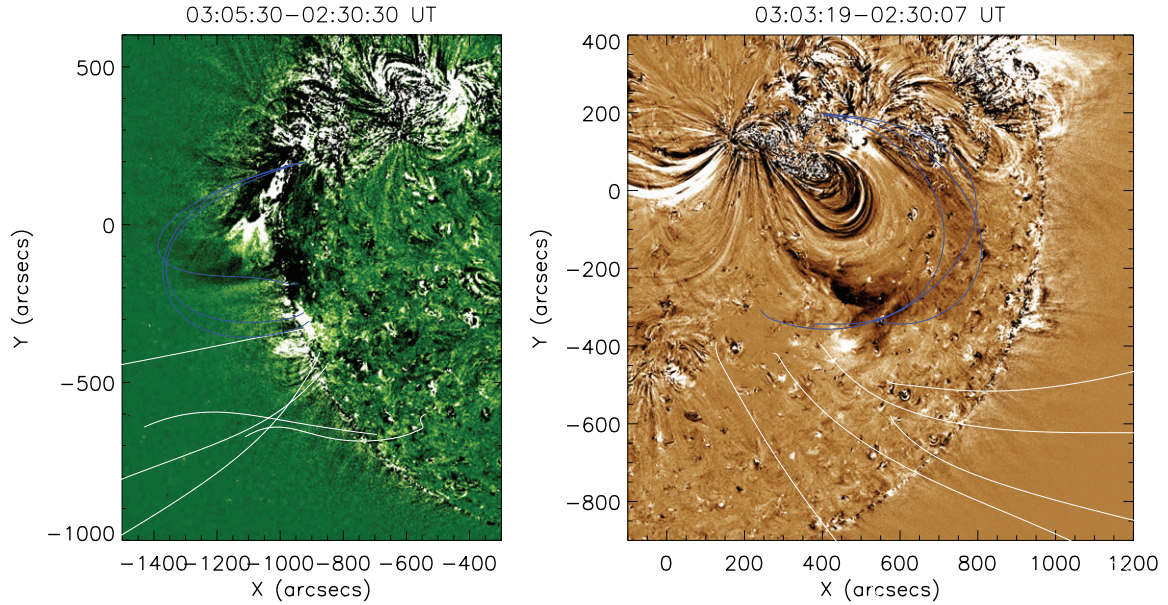
Figure 6. Difference images from EUVI-A 195 Å (left panel) and AIA 193 Å (right panel) superposed by the selected coronal magnetic field lines, which are extrapolated with the Potential Field Source-Surface model. The blue lines represent the large-scale overlying loops, and the white lines denote the open field lines from the coronal hole.

(A color version of this figure is available in the online journal.)

AIA 171 Å and continuously traveled beyond the limb. These super-fast MHD waves are different from the single-pulse EUV waves, such as the fast wave here, which freely propagate over the solar surface and can be detected in many AIA EUV channels.

As to the physical origin of the wave, our analysis is as follows: The accompanying CME opened up large-scale coronal loops that evolved into the CME front, and the wave front formed earlier than the CME front (better seen in the attached movie). The wave is unlikely to be driven by the leading CME front. In addition, the slow CME was too weak to trigger the fast wave. Thus, we exclude the CME as the possible origin. Though it is widely accepted that EUV waves are barely associated with flares, the C1.0 flare also could be the wave driver because of the almost simultaneous onset with the wave. The disadvantage for the flare is that the start point of the wave was far from the flare kernel. On the other hand, small-scale ejecta (e.g., spray surges, erupting plasmoids) could generate an initially driven shock, which travels freely after the ejection stops (Klein et al. 1999; Klassen et al. 2003; Zheng et al. 2011). Naturally, due to the close temporal and spatial relationship between the wave and the jet, it is extremely reasonable that the wave was triggered by the jet and kept freely propagating after the jet stopped.

According to Equation (5) in Patsourakos & Vourlidas (2012), we calculate the total energy $E_{\rm wave}$ for the EUV wave as follows:

$$E_{\rm wave} = (F_{\rm kin} + \Delta F_{\rm rad} + \Delta F_{\rm cond})\theta R\, dR\, dt.$$

Here, $F_{\rm kin}$, $F_{\rm rad}$, and $F_{\rm cond}$ are the kinetic flux, radiative losses flux, and coronal thermal conduction flux, respectively. The Δ quantities represent the change in the corresponding fluxes associated with the EUV wave. The EUV wave propagated in angular extent θ, the wave front had the radius R and thickness dR, and dt is the wave lifetime. $F_{\rm kin}$ can be calculated by $F_{\rm kin} = \rho(\delta I/I)^2 v_w^3/8$, with ρ being the mass density, $\delta I/I$ being the relative intensity change, and v_w being the wave speed. Taking $v_w = 1000\,{\rm km\,s^{-1}}$, $\delta I/I = 0.05$, and a typical coronal density of 5×10^8 cm^{-3} in the quiet Sun, we get

$F_{\rm kin} = 2.6 \times 10^5$ erg cm^{-2} s^{-1}. From Withbroe & Noyes (1977), we get the standard $F_{\rm rad} = 1.2 \times 10^5$ erg cm^{-2} s^{-1} and $F_{\rm cond} = 2.5 \times 10^5$ erg cm^{-2} s^{-1} in the quiet-Sun corona. For a density increase of 10%, $F_{\rm rad}$ increases by 21%. For a 7% increase in the temperature, there was a 26% increase in $F_{\rm cond}$. For the EUV wave, using the special values of $\theta = \pi/2$, $R = 120$ Mm, $dR = 25$ Mm, and $dt = 600$ s, we finally get $E_{\rm wave} = 9.5 \times 10^{27}$ erg. On the other hand, assuming its shape is a cylinder, the jet has a length of 50 Mm and a width of 26 Mm (indicated by the dotted lines in Figure 2(c)). If the density is 10^9 cm^{-3}, then the jet mass is about 4.4×10^{14} g, and we can derive its kinetic energy to be about 1.8×10^{28} erg. From the energy viewpoint, it is probable that the jet can trigger the EUV wave.

However, what is somewhat puzzling is how the fast EUV wave was driven by the slow mini-filament eruption. This makes the wave nature uncertain and leaves other possibilities open. Studying more of this kind of wave will be helpful in understanding their nature and their relation with associated eruptions. The nature and origin of EUV waves remains subtle; further observations and theoretical work will be essential.

REFERENCES

Attrill, G. D. R., Harra, L. K., van Driel-Gesztelyi, L., & Démoulin, P. 2007, ApJ, 656, L101
Biesecker, D. A., Myers, D. C., Thompson, B. J., et al. 2002, ApJ, 569, 1009
Bogdan, T. J., Carlsson, M., Hansteen, V. H., et al. 2003, ApJ, 599, 626
Cheng, X., Zhang, J., Olmedo, O., et al. 2012, ApJ, 745, L5
Chen, P. F. 2006, ApJ, 641, L153
Chen, P. F., Wu, S. T., Shibata, K., & Fang, C. 2002, ApJ, 572, L99

Cliver, E. W., Laurenza, M., Storini, M., & Thompson, B. J. 2005, ApJ, 631, 604

Cohen, O., Attrill, G. D. R., Manchester, W. B., IV., & Wills-Davey, M. J. 2009, ApJ, 705, 587

Delannée, C., Török, T., Aulanier, G., & Hochedez, J. F. 2008, Sol. Phys., 247, 123

Downs, C., Roussev, I. I., van der Holst, B., et al. 2011, ApJ, 728, 2

Fedun, V., Shelyag, S., & Erdélyi, R. 2011, ApJ, 727, 17

Gallagher, P. T., & Long, D. M. 2011, Space Sci. Rev., 158, 365

Gopalswamy, N., Yashiro, S., Temmer, M., et al. 2009, ApJ, 691, L123

Hong, J. C., Jiang, Y. C., Zheng, R. S., et al. 2011, ApJ, 738, L20

Howard, R. A., Moses, J. D., Vourlidas, A., et al. 2008, Space Sci. Rev., 136, 67

Kaiser, M. L., Kucera, T. A., Davila, J. M., et al. 2008, Space Sci. Rev., 136, 5

Klassen, A., Pohjolainen, S., & Klein, K.-L. 2003, Sol. Phys., 218, 197

Klein, K.-L., Khan, J. I., Vilmer, N., Delouis, J.-M., & Aurass, H. 1999, A&A, 346, L53

Lemen, J. R., Title, A. M., Akin, D. J., et al. 2011, Sol. Phys., 275, 17

Li, T., Zhang, J., Yang, S. H., & Liu, W. 2012, ApJ, 746, 13

Liu, W., Nitta, N. V., Schrijver, C. J., Title, A. M., & Tarbell, T. D. 2010, ApJ, 723, L53

Liu, W., Title, A. M., Zhao, J. W., et al. 2011, ApJ, 736, L13

Long, D. M., Gallagher, P. T., McAteer, R. T. J., & Bloomfield, D. S. 2008, ApJ, 680, L81

Moore, R. L., Cirtain, J. W., Sterling, A. C., & Falconer, D. A. 2010, ApJ, 720, 757

Moses, D., Clette, F., Delaboudinière, J.-P., et al. 1997, Sol. Phys., 175, 571

Ofman, L., Liu, W., Title, A., & Aschwanden, M. 2011, ApJ, 740, 33

Ofman, L., & Thompson, B. J. 2002, ApJ, 574, 440

Patsourakos, S., & Vourlidas, A. 2012, Sol. Phys., in press

Scherrer, P. H., Bogart, R. S., & Bush, R. I. 1995, Sol. Phys., 162, 129

Schrijver, C. J., & De Rosa, M. L. 2003, Sol. Phys., 212, 165

Shen, Y. D., Liu, Y., Su, J. T., & Deng, Y. Y. 2012, ApJ, 745, 2

Thompson, B. J., Gurman, J. B., Neupert, W. M., et al. 1999, ApJ, 517, L151

Thompson, B. J., Plunkett, S. P., Gurman, J. B., et al. 1998, Geophys. Res. Lett., 25, 2465

Veronig, A. M., Muhr, N., Kienreich, I. W., Temmer, M., & Vršnak, B. 2010, ApJ, 716, L157

Veronig, A. M., Temmer, M., & Vršnak, B. 2008, ApJ, 681, L113

Wang, H., Shen, C., & Lin, J. 2009, ApJ, 700, 1716

Wang, Y. M. 2000, ApJ, 543, L89

Warmuth, A. 2010, Adv. Space Res., 45, 527

Williams, D. R., Mathioudakis, M., Gallagher, P. T., et al. 2002, MNRAS, 336, 747

Wills-Davey, M. J., & Attrill, G. D. R. 2009, Space Sci. Rev., 149, 325

Wills-Davey, M. J., DeForest, C. E., & Stenflo, J. O. 2007, ApJ, 664, 556

Wills-Davey, M. J., & Thompson, B. J. 1999, Sol. Phys., 190, 467

Withbroe, G. L., & Noyes, R. W. 1977, Ann. Rev. Astron. Astrophys., 15, 363

Wu, S. T., Zheng, H. N., Wang, S., et al. 2001, J. Geophys. Res., 106, 25089

Zheng, R. S., Jiang, Y. C., Hong, J. C., et al. 2011, ApJ, 739, L39

Zheng, R. S., Jiang, Y. C., Yang, J. Y., et al. 2012, ApJ, 747, 67

Zhukov, A. N. 2011, J. Atmos. Sol.-Terr. Phys., 73, 1096

Zhukov, A. N., & Auchère, F. 2004, A&A, 427, 705